

Article

Robust Tracking Control of a Three-Phase Charger under Unbalanced Grid Conditions

Chivon Choeung¹ , Meng Leang Kry² and Young Il Lee^{2,*} 

¹ Faculty of Electrical Engineering, National Polytechnic Institute of Cambodia, Phnom Penh 12409, Cambodia; chivonchoeung@gmail.com

² Electrical and Information Engineering, Seoul National University of Science and Technology, Seoul 01811, Korea; kry_mengleang90@seoultech.ac.kr

* Correspondence: yilee@seoultech.ac.kr; Tel.: +82-02-970-6544

Received: 6 November 2018; Accepted: 30 November 2018; Published: 3 December 2018



Abstract: This paper presents a robust control technique for three-phase chargers under unbalanced grid conditions. The control method consists of inner-loop robust grid-current control and outer-loop proportional integral control for constant current (CC) and constant voltage (CV) control. A dual-current control for the inner-loop positive and negative sequence is employed to eliminate the unbalanced current caused by the grid so that a constant current and voltage can be provided to the batteries. The inner-loop robust controllers utilize state feedback with integral action in the dq -synchronous frame. A linear matrix inequality-based optimization scheme is used to determine stabilizing gains of the controllers to maximize the convergence rate to steady state in the presence of uncertainties. The uncertainties of the system are described as the potential variation range of the inductance and resistance in the L -filter.

Keywords: battery charger; fast charging; unbalanced grid; linear matrix inequality (LMI); robust control

1. Introduction

With the emergence of enormous amounts of plug-in hybrid electric vehicles (PHEVs) and electric vehicles (EVs) and the flourishing of renewable energy, the development of power storage has become an interesting topic. Therefore, the technology related to battery charging has drawn a lot of attention from governments, auto-makers, and researchers. In order to answer the demands for fast and efficient battery chargers, many control strategies have been proposed.

Classical Proportional Integral (PI) control has been proposed for single-phase chargers [1,2]. The charging scheme was designed based on constant-current (CC) and constant-voltage (CV) charging mode which provides shorter charging times compare to those of fixed voltage charging methods. However, the main drawback of PI controllers is gain tuning for both inner-loop and outer-loop controller. Furthermore, since the topology of these proposed methods is based on single-phase converters, the charging current limit is smaller compared to those of three-phase chargers.

Model predictive control (MPC) has been proposed in [3] for a bidirectional three-phase charger. This method could provide bidirectional power transfer with instantaneous mode charging capability and fast dynamic response. Even so, the charging method from power grid to vehicle is based on fixed voltage mode therefore the batteries need a longer time to be fully charged. In [4], another MPC-based control has also been proposed for a three-phase charger to charge Li-ion batteries. The controller outputs the optimum pulse width modulation (PWM) switching signal to provide the nearest output reference with fast convergence rate to the equilibrium point whose power factor is unity. However, this method requires a DC/DC converter to maintain the CC/CV charging stage. Furthermore, in unbalanced grid conditions these methods [3,4], fail to provide a constant voltage to

the batteries due to the lack of negative sequence compensator. The MPC-based control method for a three-level single-phase charger described in [5] provides a smooth and low total harmonic distortion output to the battery. However, a single-phase based topology charger cannot supply as much output current as three-phase ones.

In [6], a PI control method was used in the AC/DC converter side to maintain dc-link voltage constant while deadbeat control is used in the DC/DC converter to regulate the charging current to battery. The deadbeat control provides really fast transient response which setting time reaches the steady state in just a few sampling instants. However, it is really sensitive to the parametric uncertainty of the system and measurement noise, particularly for high sampling rates.

Most of the abovementioned methods [1,2,4,6] are using bi-directional DC/DC converters for CC/CV operation along with DC/AC inverters for power factor control and DC-link voltage control. DC/DC converter topologies have been proposed for single-phase [7,8] and three-phase chargers [9,10] to improve the charging efficiency. In [7,10], three operational modes for bidirectional chargers i.e., grid-to-vehicle (G2V), vehicle-to-grid (V2G), and vehicle-to-home (V2H) were considered to provide a full bidirectional charger capability for electric vehicles. These methods adopt classical controllers such as PI which require multi-loop gain tunings. Moreover, they did not consider how to handle unbalanced grid conditions.

In this paper, a robust tracking control of a three-phase charger under unbalanced grid conditions is proposed without using DC/DC converter as an interface between the three-phase AC/DC converter and the batteries. Therefore, the charger is smaller in size and with less component expense. The battery is charged with a constant current until the voltage reaches the recommended maximum voltage, then the voltage is maintained constant until the current consumed by battery falls to a residual value. The control method consists of inner-loop robust grid-current control and outer-loop proportional integral control for constant current (CC) and constant voltage (CV) control. A dual-current control for the inner-loop positive and negative sequence is employed to eliminate the unbalanced current caused by the grid so that a constant current and voltage can be provided to the batteries. The inner-loop robust controllers utilize state feedback with integral action in the dq -synchronous frame. A linear matrix inequality-based optimization scheme is used to determine stabilizing gains of the controllers to maximize the convergence rate to steady state in the presence of uncertainties. The uncertainties of the system are described as the potential variation range of the inductance and resistance in the L -filter. The conventional phase-locked loop (PLL) method is considered in this paper to obtain the grid voltage phase angle.

2. Battery Chargers for EVs or PHEVs

Here, a detailed charger classification is presented. As discussed in the previous section, there are a few types of battery charger topologies such as a single-phase charger, three-phase charger with front end AC/DC converter and isolated DC/DC topologies, and only three-phase AC/DC topology. EVs or PHEVs can be recharged by connecting a plug to an external power source through an AC or DC charging system. The DC charging station is an off-board charger mounted at fixed place providing required DC power directly to the batteries inside the vehicle. The charging AC outlet can be single or three-phase and inevitably needs an on-board AC/DC charger with a power factor correction. The charger classification according to Society of Automotive Engineers (SAE) EV AC Charging Power Levels is summarized in Tables 1–3 for single-phase, three-phase and DC chargers, respectively [11,12].

Table 1. Single-phase Automotive Engineers (SAE) EV AC charging power level.

Nominal Supplied Voltage (V)	Maximum Current (A)	Output Power Level (kW)
120V AC, single-phase	12	1.08
120V AC, single-phase	16	1.44
208–240 V AC, single-phase	16	3.3
208–240 V AC, single-phase	32	6.6
208–240 V AC, single-phase	≤80	≤14.4

Table 2. Three-phase SAE EV AC charging power level.

Nominal Supplied Voltage (V)	Maximum Current (A)	Output Power Level (kW)
480 V AC, three-phase	16	11
480 V AC, three-phase	80	65
480 V AC, three-phase	160	133
600 V AC, three-phase	160	166

Table 3. SAE EV DC charging power level.

Nominal Supplied Voltage (V)	Maximum Current (A)	Output Power Level (kW)
200–450 V DC	≤80	36
200–450 V DC	≤200	90
200–600 V DC	≤400	240

3. System Description

A three-phase charger is shown in Figure 1.

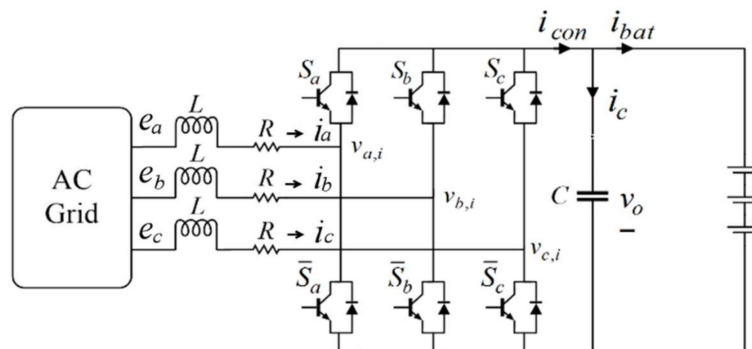


Figure 1. Three-phase bidirectional charger with L-filter.

The dynamics of the line current is expressed in the *abc*-axis as follows:

$$\begin{cases} L \frac{di_a(t)}{dt} + Ri_a(t) = e_a - v_{a,i} \\ L \frac{di_b(t)}{dt} + Ri_b(t) = e_b - v_{b,i} \\ L \frac{di_c(t)}{dt} + Ri_c(t) = e_c - v_{c,i} \end{cases} \quad (1)$$

where:

$$\begin{aligned} v_{a,i} &:= \frac{2u_a - u_b - u_c}{6} v_o(t) \\ v_{b,i} &:= \frac{-u_a + 2u_b - u_c}{6} v_o(t) \\ v_{c,i} &:= \frac{-u_a - u_b + 2u_c}{6} v_o(t) \end{aligned} \quad (2)$$

The switches operate in continuous conduction mode, where two switches in each leg of the AC/DC charger should be operated in a complementary mode to avoid short circuits. The switching states of the charger is determined by u_a, u_b or u_c as:

$$\begin{aligned} u_a &= \begin{cases} 1, & \text{when } S_a \text{ is on and } \bar{S}_a \text{ is off} \\ -1, & \text{when } S_a \text{ is off and } \bar{S}_a \text{ is on} \end{cases} \\ u_b &= \begin{cases} 1, & \text{when } S_b \text{ is on and } \bar{S}_b \text{ is off} \\ -1, & \text{when } S_b \text{ is off and } \bar{S}_b \text{ is on} \end{cases} \\ u_c &= \begin{cases} 1, & \text{when } S_c \text{ is on and } \bar{S}_c \text{ is off} \\ -1, & \text{when } S_c \text{ is off and } \bar{S}_c \text{ is on} \end{cases} \end{aligned} \tag{3}$$

It is quite challenging to control a three-phase converter in abc -frame due to its time-variant behavior, so the dq transformation is used to obtain DC like signal in dq -frame. Therefore, the dynamics (1) in abc -axis can be transformed to dq -axis as follows [13]:

$$\frac{d\mathbf{i}_{dq}(t)}{dt} = \mathbf{A}_c \mathbf{i}_{dq}(t) + \mathbf{B}_c v_o(t) \mathbf{u}(t) + \mathbf{d}_c(t) \tag{4}$$

where $\mathbf{i}_{dq}(t) := \begin{bmatrix} i_d(t) \\ i_q(t) \end{bmatrix}$, $\mathbf{u}(t) = \begin{bmatrix} u_d(t) \\ u_q(t) \end{bmatrix}$, $\mathbf{d}_c(t) = \begin{bmatrix} 0 \\ -\frac{E_m}{L} \end{bmatrix}$, $\mathbf{A}_c = \begin{bmatrix} -\frac{R}{L} & \omega \\ \omega & -\frac{R}{L} \end{bmatrix}$, $\mathbf{B}_c = \begin{bmatrix} -\frac{1}{2L} & 0 \\ 0 & -\frac{1}{2L} \end{bmatrix}$, and ω is the angular frequency of the AC voltage source.

Any unbalanced three-phase voltage can be expressed by the sum of positive, negative and zero sequence [14]. However, the three-phase charger system has only three wires therefore the zero sequence is does not exist. Hence, the unbalanced current and voltage can be expressed as:

$$\mathbf{e}_{abc} = \mathbf{e}_{abc}^p + \mathbf{e}_{abc}^n \tag{5a}$$

$$\mathbf{i}_{abc} = \mathbf{i}_{abc}^p + \mathbf{i}_{abc}^n \tag{5b}$$

The positive and negative sequence of the grid voltage are assumed to be:

$$\mathbf{e}_{abc}^p = \begin{bmatrix} e_a^p \\ e_b^p \\ e_c^p \end{bmatrix} = \frac{1}{3} \begin{bmatrix} 1 & \alpha & \alpha^2 \\ \alpha^2 & 1 & \alpha \\ \alpha & \alpha^2 & 1 \end{bmatrix} \begin{bmatrix} e_a \\ e_b \\ e_c \end{bmatrix} \tag{6a}$$

$$\mathbf{e}_{abc}^n = \begin{bmatrix} e_a^n \\ e_b^n \\ e_c^n \end{bmatrix} = \frac{1}{3} \begin{bmatrix} 1 & \alpha^2 & \alpha \\ \alpha & 1 & \alpha^2 \\ \alpha^2 & \alpha & 1 \end{bmatrix} \begin{bmatrix} e_a \\ e_b \\ e_c \end{bmatrix} \tag{6b}$$

where α and α^2 are phase-shifting operators and defined as:

$$\alpha = -\frac{1}{2} + j\frac{\sqrt{3}}{2} \text{ and } \alpha^2 = -\frac{1}{2} - j\frac{\sqrt{3}}{2} \tag{7}$$

Substituting Equation (7) into Equation (6) yields:

$$\mathbf{e}_{abc}^p = \frac{1}{3} \begin{bmatrix} 1 & -\frac{1}{2} & -\frac{1}{2} \\ -\frac{1}{2} & 1 & -\frac{1}{2} \\ -\frac{1}{2} & -\frac{1}{2} & 1 \end{bmatrix} \begin{bmatrix} e_a \\ e_b \\ e_c \end{bmatrix} + j\frac{1}{2\sqrt{3}} \begin{bmatrix} 0 & 1 & -1 \\ -1 & 0 & 1 \\ 1 & -1 & 0 \end{bmatrix} \begin{bmatrix} e_a \\ e_b \\ e_c \end{bmatrix} \tag{8a}$$

$$e_{abc}^n = \frac{1}{3} \begin{bmatrix} 1 & -\frac{1}{2} & -\frac{1}{2} \\ -\frac{1}{2} & 1 & -\frac{1}{2} \\ -\frac{1}{2} & -\frac{1}{2} & 1 \end{bmatrix} \begin{bmatrix} e_a \\ e_b \\ e_c \end{bmatrix} - j \frac{1}{2\sqrt{3}} \begin{bmatrix} 0 & 1 & -1 \\ -1 & 0 & 1 \\ 1 & -1 & 0 \end{bmatrix} \begin{bmatrix} e_a \\ e_b \\ e_c \end{bmatrix} \quad (8b)$$

An all-pass filter allows all range of frequencies to pass, however it is used to obtain the imaginary part of Equation (8) by shifting 90° from the original phase. The characteristic of the all-pass filter is validated in Figure 2a using a Bode plot and the schematic of an all-pass filter is shown in Figure 2b.

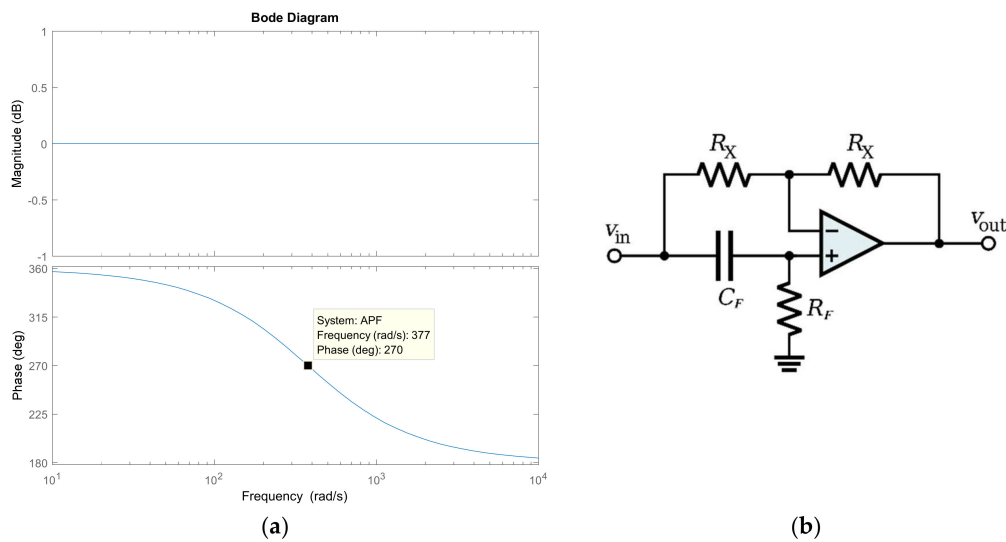


Figure 2. (a) Bode plot of an all-pass filter (b) an all-pass filter schematic.

The transfer function of the all-pass filter can be expressed as follows:

$$H(s) = \frac{1 - R_F C_F s}{1 + R_F C_F s} \quad (9)$$

The same process is used to extract positive and negative sequence of grid current and voltage. The block diagrams of positive and negative sequence extraction are shown in Figures 3 and 4, respectively.

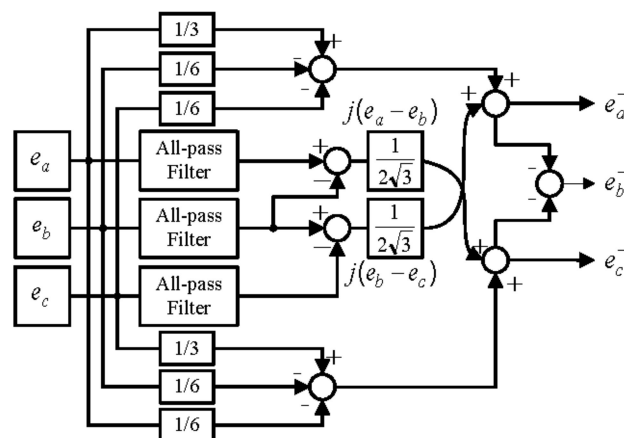


Figure 3. Positive sequence extraction block diagram.

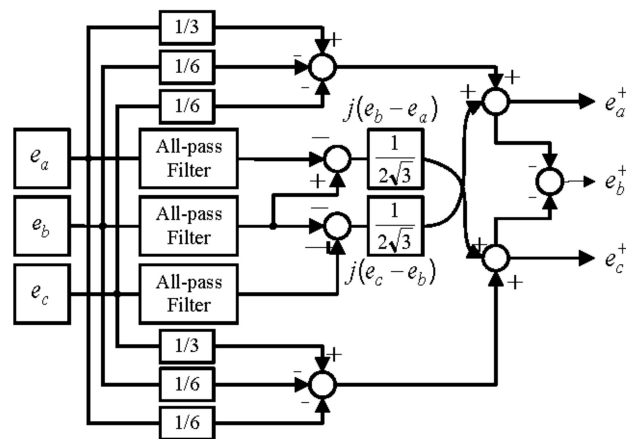


Figure 4. Negative sequence extraction block diagram.

From Equation (5), the current dynamics (4) can be rewritten as a combination of positive and negative sequence. The dynamic of both sequences is almost identical; however, the only difference is the sign of ω due to the inverse direction of the negative sequence vector rotation [15]. Then, we have:

$$\frac{d\mathbf{i}_{dq}^p(t)}{dt} = \mathbf{A}_c^p \mathbf{i}_{dq}^p(t) + \mathbf{B}_c v_o(t) \mathbf{u}_{dq}^p - \mathbf{d}_c^p(t) \tag{10a}$$

$$\frac{d\mathbf{i}_{dq}^n(t)}{dt} = \mathbf{A}_c^n \mathbf{i}_{dq}^n(t) + \mathbf{B}_c v_o(t) \mathbf{u}_{dq}^n - \mathbf{d}_c^n(t) \tag{10b}$$

where $\mathbf{A}_c^p := \begin{bmatrix} -\frac{R}{L} & \omega \\ -\omega & -\frac{R}{L} \end{bmatrix}$, $\mathbf{A}_c^n := \begin{bmatrix} -\frac{R}{L} & -\omega \\ \omega & -\frac{R}{L} \end{bmatrix}$, $\mathbf{B}_c := \begin{bmatrix} -\frac{1}{2L} & 0 \\ 0 & -\frac{1}{2L} \end{bmatrix}$, $\mathbf{d}_c^p := \begin{bmatrix} 0 \\ \frac{e_q^p}{L} \end{bmatrix}$, $\mathbf{d}_c^n := \begin{bmatrix} 0 \\ \frac{e_q^n}{L} \end{bmatrix}$ \mathbf{i}_{dq} and \mathbf{u}_{dq} are the grid current and control input in dq -frame, respectively. The output voltage $v_o(t)$ is governed by the following dynamic equation:

$$C \frac{dv_o(t)}{dt} = i_{con}(t) - i_{bat}(t) \tag{11}$$

where:

$$i_{con}(t) = \frac{3}{4} \mathbf{i}_{dq}^T(t) \mathbf{u}(t) \tag{12}$$

and i_{con} is the converter current and i_{bat} is an output current to the battery.

Model (10) can be transformed in the following discrete-time system with sampling time h :

$$\mathbf{x}^p(k+1) = \mathbf{A}^p \mathbf{x}^p(k) + \mathbf{B} v_o(k) \mathbf{u}^p(k) - \mathbf{d}^p(k) \tag{13a}$$

$$\mathbf{x}^n(k+1) = \mathbf{A}^n \mathbf{x}^n(k) + \mathbf{B} v_o(k) \mathbf{u}^n(k) - \mathbf{d}^n(k) \tag{13b}$$

where $\mathbf{A}^{pn} = \mathbf{I}_{4 \times 4} + \mathbf{A}_c^{pn}$, $\mathbf{B} = \mathbf{B}_c h$, $\mathbf{d}^{pn} = \mathbf{d}_c^{pn} h$, $\mathbf{x}^{pn} = \mathbf{i}_{dq}^{pn}$.

4. Robust Controller Design

In this section, the uncertainties model of the system, offset-free control and robust optimal gain are discussed. Suppose that the value of L and R in each phase are equal but vary in certain ranges as indicated below:

$$L_1 \leq L \leq L_2 \tag{14a}$$

$$R_1 \leq R \leq R_2 \tag{14b}$$

Here, we denote the matrices (A , B) corresponding to the four possible combinations of the immoderate value of $1/L$ and $1/R$ as (A_i , B_i) ($i = 1, 2, 3, 4$) and suppose that the matrices (A , B) belongs to the polytopic uncertain set Ψ below:

$$\Psi = \left\{ \sum_{n=1}^4 \mu_n (A_i, B_i) \mid \sum_{n=1}^4 \mu_n = 1, \mu_n \geq 0 \right\} \quad (15)$$

The uncertainties of the system can be any kind of variation, but should lies within the range (14). The system uncertain range can be determined as:

$$L_{nom} / \mu \leq L \leq \mu L_{nom} \quad (16a)$$

$$R_{nom} / \mu \leq R \leq \mu R_{nom} \quad (16b)$$

where R_{norm} and L_{norm} are nominal value of the filter resistance and inductance, respectively, and μ (>1) can be considered as a tuning parameter.

In consideration of compensating the offset error despite the system's uncertainty model, the control law based on [16] is employed for Equation (13):

$$\begin{cases} \mathbf{g}^p(k) = \mathbf{g}^p(k+1) + (\mathbf{x}_{ref}^p - \mathbf{x}^p(k-1)) \\ \mathbf{u}^p(k) = \mathbf{K}^p \mathbf{x}^p(k) + \mathbf{L}^p \mathbf{g}^p(k) \end{cases} \quad (17a)$$

$$\begin{cases} \mathbf{g}^n(k) = \mathbf{g}^n(k+1) + (\mathbf{x}_{ref}^n - \mathbf{x}^n(k-1)) \\ \mathbf{u}(k) = \mathbf{K}^n \mathbf{x}^n(k) + \mathbf{L}^n \mathbf{g}^n(k) \end{cases} \quad (17b)$$

where \mathbf{K}^{pn} and \mathbf{L}^{pn} are state feedback and integrator gains, respectively. Because of the integrator in Equation (17), the steady-state error between the reference state \mathbf{x}_{ref}^{pn} and the grid-current \mathbf{x}^{pn} will be compensated provided that the closed-loop system is stable.

In order to eliminate the unbalanced current caused by negative sequence and provide a constant charging current and voltage to the batteries, the reference state should be given as:

$$\mathbf{x}_{ref}^{pn} := \begin{bmatrix} x_{dref}^p \\ x_{qref}^p \\ x_{dref}^n \\ x_{qref}^n \end{bmatrix} = \begin{bmatrix} 0 \\ i_{qref}^p \\ 0 \\ 0 \end{bmatrix} \quad (18)$$

where $x_{qref}^p = i_{qref}^p$ is generated by the outer-loop controller depending on its CC and CV control objectives.

The same process is used to find optimal gains for positive and negative sequence, so the procedure is unified. A systematic design method was proposed in [17] to obtain stabilizing state feedback gain \mathbf{K} and integral gain \mathbf{L} of Relation (17) using LMI. From relation (13) and (17), we get:

$$\mathbf{z}(k+1) = \mathbf{A}_a \mathbf{z}(k) + \mathbf{B}_a \mathbf{u}(k) + \mathbf{D}(k) \quad (19)$$

$$\text{where } \mathbf{z}(k) := \begin{bmatrix} \mathbf{x}(k) \\ \mathbf{g}(k) \end{bmatrix}, \mathbf{A}_a := \begin{bmatrix} \mathbf{A} & \mathbf{0}_{2 \times 2} \\ -\mathbf{C} & \mathbf{I}_{2 \times 2} \end{bmatrix}, \mathbf{B}_a := \begin{bmatrix} \mathbf{B} \\ \mathbf{0}_{2 \times 2} \end{bmatrix}, \mathbf{C} = \begin{bmatrix} 1 & 0 \\ 0 & 1 \end{bmatrix}, \mathbf{D}(k) := \begin{bmatrix} \mathbf{d}(k) \\ \mathbf{x}_{ref} \end{bmatrix}.$$

The control input $\mathbf{u}(k)$ can be rewritten as:

$$\mathbf{u}(k) = \mathbf{Fz}(k) \mathbf{F} := \begin{bmatrix} \mathbf{K} & \mathbf{L} \end{bmatrix} \quad (20)$$

Assume that $D(k) = 0$ to determine stabilizing gain F , then the closed-loop system can be obtained as follows:

$$z(k+1) = (A_a + B_a F)z(k) \quad (21)$$

The closed-loop dynamic (21) stable if there exists a positive-definite matrix W such that:

$$W - (A_a + B_a F)^T W (A_a + B_a F) > 0 \quad (22)$$

It is obvious that the condition (22) holds for some $W_0 > 0 (W_0 < W)$

$$W_0 - (A_a + B_a F)^T W (A_a + B_a F) > 0 \quad (23)$$

By applying Schur complement and uncertain set Equation (15) to Equation (22), we get [17]

$$\begin{bmatrix} S_0 & S_0^T A_{ai}^T + H^T B_{ai}^T \\ A_{ai} S_0 + B_{ai} H & S \end{bmatrix} > 0, \quad (i = 1, \dots, 4), \quad (24)$$

where $H := FS_0$, $S = W^{-1}$, $S_0 := S_0^{-1}$, $A_{ai} := \begin{bmatrix} A_i & 0_{2 \times 2} \\ -C & I_{2 \times 2} \end{bmatrix}$, $B_{ai} := \begin{bmatrix} B_i \\ 0_{2 \times 2} \end{bmatrix}$, $(i = 1, 2, 3, 4)$.

To summarize, closed-loop system Equation (22) is asymptotically stable if there exist symmetric positive definite matrices S and S_0 and a matrix H such that Equation (24) holds and the stabilizing gain is given as:

$$F = HS_0^{-1} \quad (25)$$

Assume that $W_0 < \alpha W$ or equivalent to

$$S < \alpha S_0 (0 < \alpha < 1) \quad (26)$$

It can be expected that a small α would give a fast convergence of z to the origin. Therefore, to obtain optimal gain F such that the convergence time is minimized, the following optimization problem should be solved:

$$\begin{aligned} & \text{Minimize } \alpha \text{ subject to (24) and (26)} \\ & S, S_0 > 0, \\ & \alpha > 0, H \end{aligned} \quad (27)$$

This optimization scheme is a generalized eigenvalue problem [18] which can be solve efficiently by the MATLAB 2014a LMI Toolbox YALMIP solver (MathWorks, Natick, MA, USA). The implementation of (27) can be done by following the YALMIP manual and it can be found on the YALMIP website (www.yalmip.github.io).

5. Dual-Loop Charging Control

In order to perform the battery charging process, most of the battery manufacturers recommend two charging stage i.e., constant current (CC) mode followed by constant voltage (CV) mode. The battery is charged with constant current until the voltage reaches the recommended maximum voltage, then the voltage is maintained constant until the current consumed by the battery falls to a residual value. The dual-loop control strategy will be adopted for these two charging states i.e., an outer-loop controller generates proper $x_{qref}^p = i_{qref}^p$ depending on its CV or CC control objectives and the inner-loop controller (17) drives the state of x^{pn} in (13) to follow x_{ref}^{pn} .

5.1. Constant Voltage (CV) Charging Mode

Here, the outer-loop PI control for constant voltage charging is discussed. Let I_r be the output of the outer-loop control, i.e.:

$$I_r(t) = K_p(v_o^{ref} - v_o(t)) + K_i \int (v_o^{ref} - v_o(t))dt \quad (28)$$

where v_o^{ref} is the constant voltage reference for battery charge and $v_o(t)$ is the output voltage. Suppose that the dynamics of the inner-loop control in previous section is considerably fast so that we can assume:

$$i_{con}(t) \approx I_r(t) \quad (29)$$

for some current reference $I_r(t)$. From Equations (11) and (29), we get:

$$C \frac{dv_o(t)}{dt} = K_p(v_o^{ref} - v_o(t)) + K_i \int (v_o^{ref} - v_o(t))dt - i_{bat}(t) \quad (30)$$

or:

$$C \frac{d^2v_o(t)}{dt^2} + K_p \frac{dv_o(t)}{dt} + K_i v_o(t) = K_i v_o^{ref}. \quad (31)$$

The K_i and K_p gain can be determined by considering the characteristic polynomial of Equation (31) and can be given as:

$$\Delta(s) = s^2 + 2\zeta\omega_r s + \omega_r^2 \quad (32)$$

or some appropriate value of ζ and ω_r^2 ; we get:

$$K_i = \omega_r^2 \quad (33)$$

$$K_p = 2\zeta\omega_r. \quad (34)$$

The control diagram of the constant voltage control of the three-phase charger is shown in Figure 5. The battery voltage is fed-back to the out-loop controller, which produces a reference current $x_{qref}^p = i_{qref}^p$.

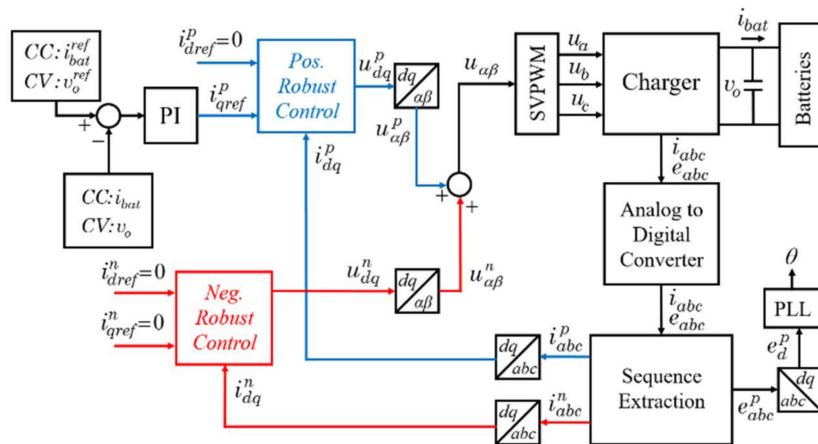


Figure 5. Control structure of the proposed method.

5.2. Constant Current (CC) Charging Mode

In constant current charging stage, the battery pack is charged with a fixed current until the voltage reaches the recommended maximum voltage, then switches to a constant voltage charging

stage. For the control of this constant current charging mode, an outer-loop PI is utilized to generate a reference signal $x_{qref}^p = i_{qref}^p$ for inner-loop robust control with the same concept as CV charging discussed in previous section. The control structure of the proposed CC charging control is validated as shown in Figure 5.

6. Simulation Results

This section presents the results of the simulation to verify the proposed method. The simulation is implemented using MATLAB 2014a LMI toolbox (YALMIP solver) to obtain robust gain for the inner-loop controller. After receiving the optimal gains from MATLAB, the controllers were applied using PSIM simulation tool. The parameters of the system are shown in Table 4. The control algorithm is conducted using a DLL block from Microsoft Visual Studio and the sampling rate is set to 10 kHz. The 3-RC equivalent circuit of Figure 6 [18,19] is used for the simulation studies. The values of parameters are determined as $R_0 = 0.01 \Omega$, $R_{d1} = R_{d2} = R_{d3} = 0.001 \Omega$, and $C_{d1} = C_{d2} = C_{d3} = 1000 F$ with $V_{bat} = 420 V$.

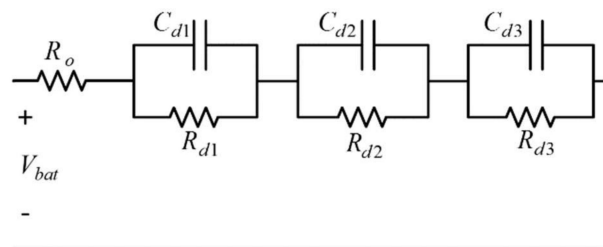


Figure 6. Battery equivalent circuit.

The implementation of the proposed control strategy can be summarized as follows:

- Step 1: Derive the discrete-time model for based on Relation (13) using nominal value of inductance L and resistance R .
- Step 2: Choose an initial uncertainty range of the parameters Relation (14), e.g., $\mu = 1.1$, and corresponding set Ψ .
- Step 3: Compute the state feedback gain K^{pn} and integrator gain L^{pn} for both positive and negative sequences by solving the optimization problem (26) using YALMIP LMI solver.
- Step 4: Implement the inner-loop current control Relation (17) to the charger.
- Step 5: If the closed-loop system shows serious overshoot or becomes unstable, then adjust the uncertainty range; i.e., raise the value of μ and repeat the procedure from Step 3.
- Step 6: After the closed-loop system becomes stable, then apply the outer-loop control for CC or CV.

Table 4. Simulation parameters.

Parameter	Value
DC-Link capacitor	4700 μF
Filter resistance	0.1 Ω
Filter inductance	5 mH
Sampling rate	10 kHz
Constant current reference	5 A
Constant voltage reference	450 V

Here, the simulation performances of the proposed charger are discussed. Figure 7a shows an unbalanced input three-phase grid-voltage supplied to charger in CC charging mode. In Figure 7b, the charger is still able to provide a considerable constant current even under unbalanced grid-voltage thanks to the its negative sequence compensator.

The CV charging mode is validated in Figure 8. We can see that the transient response of the battery voltage in CV mode is fast and constant even the three-phase input is unbalance as shown in Figure 8b.

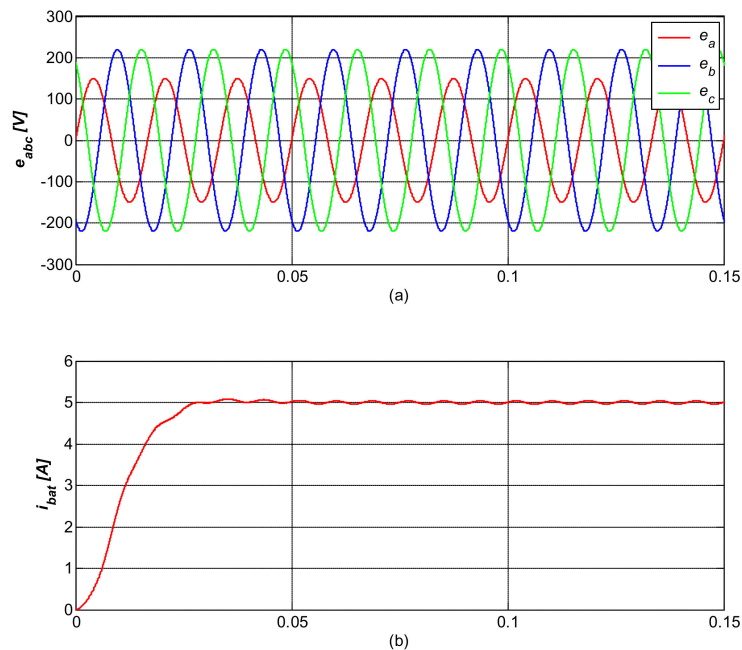


Figure 7. (a) Unbalanced input voltage (b) transient performance of battery current in constant current (CC) charging mode.

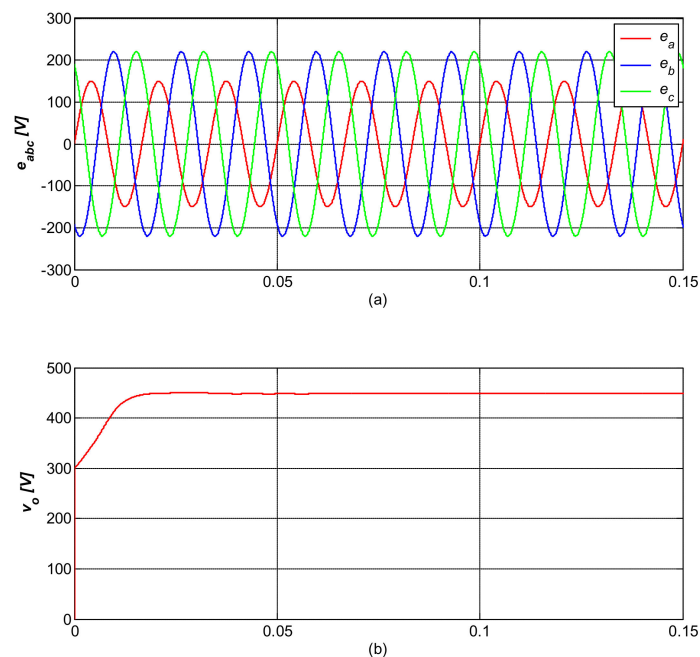


Figure 8. (a) Unbalanced input voltage (b) transient performance of battery voltage in constant voltage (CV) charging mode.

Let us discuss the comparison between the controller with and without negative sequence compensator in Figures 9 and 10, respectively. It can be noted that the controller with negative sequence compensator performs well under unbalanced input grid-voltage conditions. Both the battery current and three-phase grid-current are remarkably acceptable, as shown in Figure 9b,c, respectively. In Figure 10, the simulation performance of the controller without negative sequence

compensator is shown. Its performances, however, are not good compared to those of controller with sequence controller. It can be noted that the battery is has high oscillation and the grid-current does not show an appropriate waveform.

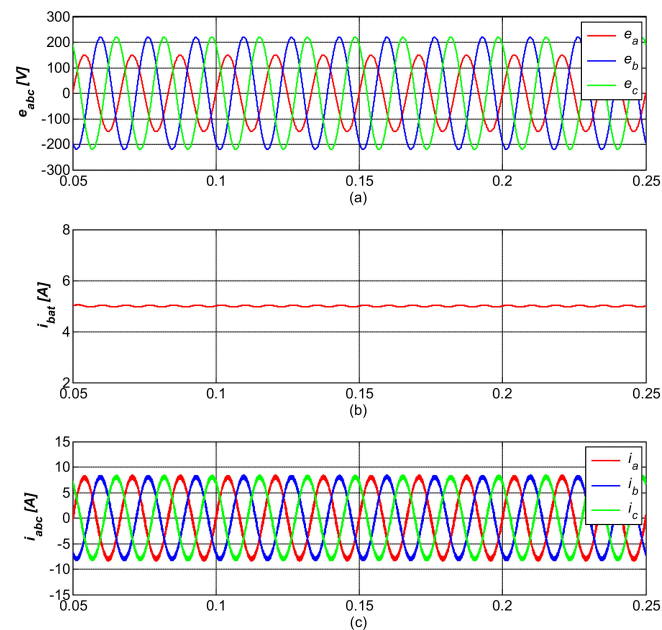


Figure 9. Steady-state performances of (a) input voltage, (b) battery current and (c) grid current; with negative sequence compensator in CC mode.

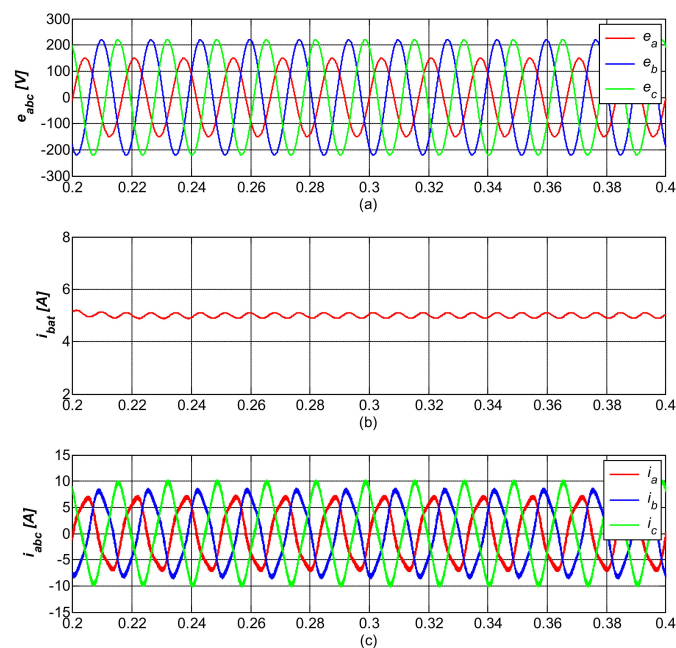


Figure 10. Steady-state performances of (a) input voltage, (b) battery current and (c) grid current; without negative sequence compensator in CC mode.

Figure 11 compares the output power of the proposed method with negative sequence compensator (Figure 11c), and without negative sequence compensator (Figure 11b). It is obvious to see that the proposed method provides a considerably constant output power to the batteries even under unbalanced grid conditions. On the other hand, it can be seen that without negative sequence compensator the charger fails to provide a constant power to the batteries. The output

power is oscillating with double the system frequency which is not good considering the battery health conditions.

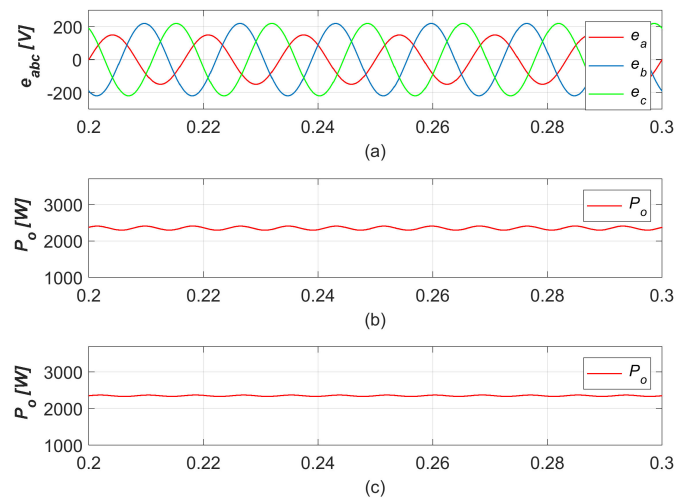


Figure 11. Steady-state performances of (a) input voltage, (b) output power without negative sequence compensator (c) output power with negative sequence compensator in CC mode.

In Figure 12, the robustness of the proposed control method is validated. As it is shown in Figure 12a–c, the control method is implemented using a nominal value of the L -filter as shown in Table 4. The grid and charger output current perform really well, with real smoothness and symmetry although the phase-a grid-voltage drops to a certain level. To test the robustness of the proposed controller, the nominal value of L -filter is changed but works under the same robust stabilizing gains. The value of the inductance and resistance are reduced by half ($\times 0.5$) which are 2.5 mH and 0.05 Ω , respectively. From Figure 12d–f, it can be seen that the charger provides almost identical constant output current as the one with nominal value. It can be assumed that the controller works pretty well under the uncertainty of the L -filter's parameters.

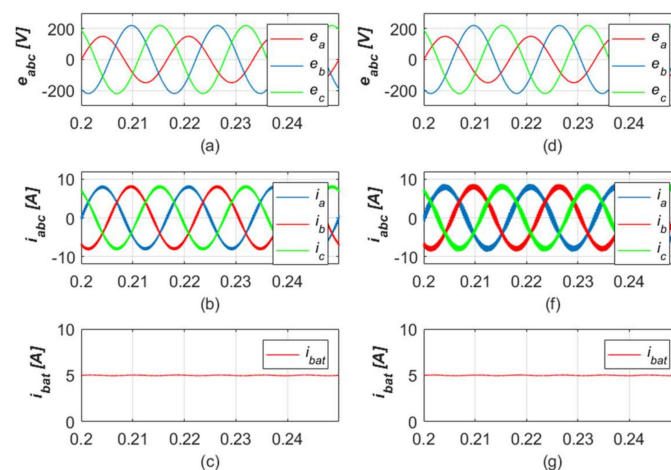


Figure 12. Steady-state performances of (a) input voltage, (b) grid current and (c) battery current with nominal L -filter value; and (d) input voltage, (e) grid current and (f) battery current with $0.5\times$ nominal L -filter value.

7. Conclusions

This paper proposes a robust control strategy for a three-phase charger under unbalanced grid conditions. The control method consists of inner-loop robust grid-current control and outer-loop proportional integral control for constant current (CC) and constant voltage (CV) control. A paralleled

current control for the inner-loop positive and negative sequence is employed to eliminate the unbalanced current caused by the grid so that a constant current and voltage can be provided to the batteries. The simulation results show that the proposed controller can provide a remarkable charging performance to the battery under unbalanced grid conditions. Moreover, the charger is able to supply a constant output power to the battery which results in better health conditions, even with an unsymmetrical voltage source. The robustness of the proposed method has been verified using parametric uncertainty of the L -filter. From an economic viewpoint, the proposed charger topology does not require an isolated DC/DC converter which leads to less component expense and a smaller installation size.

Author Contributions: Conceptualization, Y.I.L. and C.C.; Methodology, Y.I.L. and C.C.; Software, C.C.; Validation, C.C. and M.L.K.; Formal Analysis, C.C.; Investigation, C.C.; Resources, C.C. and M.L.K.; Data Curation, M.L.K.; Writing—Original Draft Preparation, C.C.; Writing—Review & Editing, C.C.; Visualization, M.L.K.; Supervision, Y.I.L.; Project Administration, Y.I.L.; Funding Acquisition, Y.I.L.

Funding: This research was funded by Seoul National University of Science and Technology grant number 2017-0793.

Conflicts of Interest: The authors declare no conflicts of interest.

Abbreviations

PLL	phase locked loop
CC	constant current
CV	constant voltage
LMI	linear matrix inequality
EV	electric vehicle
PHEV	plug-in hybrid electric vehicle
PWM	pulse width modulation
PI	proportional integral control
MPC	model predictive control

Subscripts

abc	signal in abc -frame
dq	signal in dq -frame
c	continuous time signal

Superscripts

p	signal of positive sequence
n	signal of negative sequence
T	transpose of matrix
ref	reference signal

Notations

L	filter inductance
R	filter resistance
v_o	output voltage
i_{con}	converter current
i_{bat}	output current
i_c	capacitor current
$v_{abc,i}$	pole-voltage in abc -frame
L_1	lower range of inductance
L_2	upper range of inductance

R_1	lower range of resistance
R_2	upper range of resistance
h	sampling time
g	integrator state
z	augmented state of x and g
u	control input
W	weighting matrix
K_i	integrator gain
K_p	proportional gain
C_F	all-pass filter capacitance
R_F	all-pass filter resistance
R_x	all-pass filter feedback resistance
L_{nom}	nominal value of L -filter inductance
R_{nom}	nominal value of L -filter resistance
μ	uncertainty range
Ψ	uncertainty set
K	state feedback gain
L	integrator gain
F	stabilizing gain
x	state of the system

References

- Pinto, J.G.; Monteiro, V.; Goncalves, H.; Exposto, B.; Pedrosa, D.; Couto, C.; Afonso, J.L. Bidirectional battery charger with Grid-to-Vehicle, Vehicle-to-Grid and Vehicle-to-Home technologies. In Proceedings of the IECON 39th Annual Conference of the IEEE Industrial Electronics Society, Vienna, Austria, 10–13 November 2013.
- Zhou, X.; Wang, G.; Lukic, S.; Bhattacharaya, S.; Huang, A. Multi-function bi-directional battery charger for plug-in hybrid electric vehicle application. In Proceedings of the Energy Conversion Congress and Exposition, San Jose, CA, USA, 20–24 September 2009.
- Parvez, M.; Mekhilef, S.; Tan, N.M.L.; Akagi, H. Model predictive control of a bidirectional AC-DC converter for V2G and G2V applications in electric vehicle battery charger. In Proceedings of the Transportation Electrification Conference and Expo, Dearborn, MI, USA, 15–18 June 2014.
- Lim, J.S.; Lee, Y.L. Model Predictive Control of Current and Voltage for Li-Ion Battery Charger using 3-Phase AC/DC Converter. In Proceedings of the SICE Annual Conference, Taipei, Taiwan, 18–21 August 2010.
- Monteiro, V.; Meléndez, A.A.N.; Couto, C.; Afonso, J.L. Model Predictive Current Control of a Proposed Single-Switch Three-Level Active Rectifier Applied to EV Battery Chargers. In Proceedings of the IECON—42nd Annual Conference of the IEEE Industrial Electronics Society, Florence, Italy, 23–26 October 2016.
- Gallardo-Lozano, J.; Milanés-Montero, M.I.; Guerrero-Martínez, M.A.; Romero-Cadaval, E. Electric vehicle battery charger for smart grids. *Electr. Power Syst. Res.* **2012**, *90*, 18–29. [[CrossRef](#)]
- Kwon, M.; Choi, S. An Electrolytic Capacitorless Bidirectional EV Charger for V2G and V2H Applications. *IEEE Trans. Power Electron.* **2017**, *32*, 6792–6799. [[CrossRef](#)]
- Wajahat, U.K.T.; Saad, M.; Mutsuo, N. A Transformerless Reduced Switch Counts Three-Phase APF-assisted Smart EV Charger. In Proceedings of the IEEE APEC, Tampa, FL, USA, 26–30 March 2017.
- Wang, S.; Jiang, C.; Teng, H.; Bai, H.; Kirtley, J.L., Jr. Power-Loss Analysis and Efficiency Maximization of a Silicon-Carbide MOSFET-Based Three-Phase 10-kW Bidirectional EV Charger Using Variable-DC-Bus Control. *IEEE J. Emerg. Sel. Top. Power Electron.* **2016**, *4*, 880–892. [[CrossRef](#)]
- Hu, K.; Yi, P.; Liaw, C. An EV SRM Drive Powered by Battery/Supercapacitor with G2V and V2H/V2G Capabilities. *IEEE Trans. Ind. Electron.* **2015**, *62*, 4714–4727. [[CrossRef](#)]
- Surface Vehicle Recommended Practice J1772, SAE Electric Vehicle and Plug in Hybrid Electric Vehicle Conductive Charge Coupler*; SAE International: Warrendale, PA, USA, 2010.

12. Williamson, S.S.; Rathore, A.K.; Musavi, F. Industrial Electronics for Electric Transportation Current State-of-the-Art and Future Challenges. *IEEE Trans. Ind. Electron.* **2015**, *62*, 3021–3032. [[CrossRef](#)]
13. Kim, S.K.; Choi, D.K.; Lee, K.B.; Lee, Y.I. Offset-Free Model Predictive Control for the Power Control of Three-Phase AC/DC Converters. *IEEE Trans. Ind. Electron.* **2015**, *62*, 7114–7126. [[CrossRef](#)]
14. Ma, K.; Chen, W.; Liserre, M.; Blaabjerg, F. Power Controllability of a Three-Phase Converter with an Unbalanced AC Source. *IEEE Trans. Ind. Electron.* **2015**, *30*, 1591–1604. [[CrossRef](#)]
15. Choeung, C.; Park, S.H.; Koh, B.K.; Lee, Y.I. Robust Tracking Control of a Three-Phase DC-AC Inverter for UPS Application under Unbalanced Load Conditions. In Proceedings of the IFAC Workshop on Control of Transmission and Distribution Smart Grids, Prague, Czech Republic, 11–13 October 2016.
16. Lim, J.S.; Park, C.; Han, J.; Lee, Y.I. Robust Tracking Control of a Three-Phase DC-AC Inverter for UPS Applications. *IEEE Trans. Ind. Electron.* **2014**, *61*, 4142–4151. [[CrossRef](#)]
17. Boyd, S.C.; Ghaoui, L.E.; Feron, E.; Balakrishnan, V. *Linear Matrix Inequalities in System and Control Theory*; SIAM: Philadelphia, PA, USA, 1994.
18. He, H.; Xiong, R.; Fan, J. Evaluation of Lithium-Ion Battery Equivalent Circuit Models for State of Charge Estimation by an Experimental Approach. *Energies* **2011**, *4*, 582–598. [[CrossRef](#)]
19. Nejad, S.; Gladwin, D.T.; Stone, D.A. A systematic review of lumped-parameter equivalent circuit models for real-time estimation of lithium-ion battery states. *J. Power Sources* **2016**, *316*, 183–196.



© 2018 by the authors. Licensee MDPI, Basel, Switzerland. This article is an open access article distributed under the terms and conditions of the Creative Commons Attribution (CC BY) license (<http://creativecommons.org/licenses/by/4.0/>).